AudioGuard: Omnidirectional Indoor Intrusion Detection using Audio Device

Tianben Wang

Northwest A&F University, China, wangtb@nwafu.edu.cn

Zhangben Li

Northwest A&F University, China, lzb996@nwafu.edu.cn

Honghao Yan

Northwest A&F University, China, yanhonghao9@163.com

Xiantao Liu

Northwest A&F University, China, liuxt@nwafu.edu.cn

Boqin Liu

Northwest A&F University, China, boqinliu_lbq@163.com

Shengjie Li

JD.com, Inc.,China, lishengjie@pku.edu.cn

Zhongyu Ma

Northwest Normal University, China, mazybg@nwnu.edu.cn

Jin Hu

Northwest A&F University, China, hujin007@nwsuaf.edu.cn

Daqing Zhang

Peking University, China, dqzhang@sei.pku.edu.cn

Tao Gu

Macquarie University, Australia, tao.gu@mq.edu.au

Indoor intrusion detection is a critical task for home security. Previous works in intrusion detection suffer from the problems such as blind spots in non-line-of-sight (NLOS) areas, restricted device locations, massive offline training required, and privacy concern. In this paper, we design and implement an omnidirectional indoor intrusion detection system, named *AudioGuard*, using only a pair of speaker and microphone. *AudioGuard* is able to detect both line-of-sight (LOS) and NLOS intrusions. Our observation of acoustic signal propagation in an indoor environment shows that there exist abundant multipath reflections and human movement introduces Doppler shift in echo signals. We hence capture periodical Doppler shift caused by intruder's walking motion to detect intrusion. Specifically, we first extract the Doppler shift embedded in echo signals, we then propose a periodicity polarization method to cancel out the impact of the change of radial angle and the distance on periodicity of Doppler shift. Finally, we detect intrusion by measuring periodicity of Doppler shift over time. Extensive experiments show that *AudioGuard* achieves a miss report rate of 0% and 1.75% for LOS and NLOS intrusion, respectively, and a false alarm rate of 4.17%.

CCS CONCEPTS • Human-centered computing→Ubiquitous and mobile computing→Ubiquitous and mobile computing systems and tools

Additional Keywords and Phrases: Indoor Intrusion Detection, Acoustic Sensing, Periodic Doppler shift

ACM Reference Format:

First Author's Name, Initials, and Last Name, Second Author's Name, Initials, and Last Name, and Third Author's Name, Initials, and Last Name. 2018. The Title of the Paper: ACM Conference Proceedings Manuscript Submission Template: This is the subtitle of the paper, this document both explains and embodies the submission format for authors using Word. In Woodstock '18: ACM Symposium on Neural Gaze Detection, June 03–05, 2018, Woodstock, NY. ACM, New York, NY, USA, 10 pages. NOTE: This block will be automatically generated when manuscripts are processed after acceptance.

1 INTRODUCTION

Indoor intrusion (someone enters the room without permission) detection plays a crucial role in home security such as protecting assets and preventing personal attacks. A recent report in SafeAtLast [36] shows that there are 2.5 million burglaries per year, and 66% of which are home break-ins, causing more than US$3.1 billion in damages every year. More than 25% of those who interrupt burglars become victims of violent crimes. Homes without a security system have a 300% more chance of getting broken into. The high incidence of home burglary demands effective intrusion detection in home settings.

Video-based surveillance [7-10] has been widely used to detect intrusion in public places. However, video-based approach may arise severe privacy concern when applied to a home setting. Additionally, video-based systems fail to detect NLOS intrusion. Infrared-based approaches [11-14] have been well studied over a decade. However, these systems typically have a limited sensing range since sensors are deployed in each typical entrance such as main entrance and window. In addition, these sensors need to be properly installed by well-trained professionals due to the strict requirement of sensor direction. Ultrasonic sensor approaches [33,34] may suffer the same problem.

Radar-based approaches [15-17] have been proposed in recent years. Although these approaches can achieve accurate intrusion detection, they typically require expensive human efforts in offline training and radar hardware is usually costly, hence limiting its applicability in home settings. For a cost-effective solution, WiFi devices have been used to build intrusion detection systems. These approaches [2,18-22,26-29] share the same idea of extracting Receive Signal Strength Indicator (RSSI) or Channel State Information (CSI) variation pattern and applying machine learning algorithms for pattern matching. These approaches rely heavily on massive data for offline training. To overcome data dependency, studies in [23,24] detect intrusion by comparing RSSI variance to specific threshold. However, RSSI variance varies significantly with respect to distance, location and walking direction, hence setting an accurate threshold is not feasible. Li et al [30-32] detect intrusion by identifying the transient moment of an intruder entering house with accurate estimation WiFi sensing boundary. However, WiFi-based approaches requires the transmitter and receiver placed at two sides of an intruder, else the performance declines significantly.

The audio devices embedded in smartphone have been used to detect intrusion by detecting door opening and closing events [35]. Microphone array has been used to detect intrusion [1,3]. However, like radar- and WiFi-based approaches, they rely heavily on massive data for offline training to cover all the possible conditions. Ultrasonic sensors also have been used to build intrusion detection systems [33,34]. Due to strong directionality, ultrasonic sensors-based approaches suffer the same problem as in the infrared-based approaches. Zieger et al [4] and Zu et al [38] proposed to extract various time and domain features of the data received by microphone array to identify intrusion. However, the experience-based method suffers from poor environment adaptation.

In this paper, we design and implement *AudioGuard*, an omnidirectional indoor intrusion detection system using only a pair of speaker and microphone. The system is able to detect both LOS and NLOS intrusions. *AudioGuard* can be

implemented on different audio device and is robust against interference and transceiver's location and orientation. We observe that there exist abundant acoustic reflections in an indoor environment, and intruder's walking motion always introduces a periodic Doppler shift. We hence discover our basic idea to capture intruder's walking motion which is inevitable during intrusion. By measuring the periodic Doppler shift embedded in echo signals, we can detect intrusion. Designing and implementing such an omnidirectional intrusion detection system however entails two main challenges:

1) Different from the shift of main peak of echo spectrum as explained in the classical Doppler effect theory, due to multipath reflections in indoor environments, the Doppler shift caused by walking motion appears as sidelobes of echo spectrum without obvious peak. This raises a problem of how to quantify the Doppler shift.

2) Although limbs swing during walking is periodic, as the change of radial angle and the distance from intruder to device, the Doppler shift over time embeds with nonlinear trend and its amplitude varies nonlinearly. It seriously decreases the periodicity of Doppler shift and makes it difficult to distinguish intrusion and interference, e.g., curtain fluttering.

To address the aforementioned challenges, we first propose to capture Doppler shift using echo power spectrum density (PSD) difference vector. We then propose a periodicity polarization method to cancel out the impact of the change of radial angle and the distance on Doppler shift periodicity. Finally, we detect intrusion by measuring the periodicity of Doppler shift sequence. The demo video is available at https://tinyurl.com/4y44pdbk or https://youtu.be/iI-Pk4st75o.

The main contributions of this paper are summarized as follows:

1) We design and implement *AudioGuard*, an omnidirectional intrusion detection system using only a pair of speaker and microphone. It captures both LOS and NLOS intrusions. We propose to capture Doppler shift using PSD difference vector and cancel out the impact of the change of radial angle and the distance on Doppler shift over time using a periodicity polarization algorithm. It enlarges the Doppler shift periodicity difference between walking and other movement interference.

2) We conduct extensive experiments to evaluate *AudioGuard* with a variety of indoor settings. Experiments show that *AudioGuard* can be implemented on different audio device and robust against the variation of transceiver's location and orientation. *AudioGuard* achieves a miss report rate of 0% and 1.75% for LOS and NLOS intrusion, respectively. The false alarm rate under interference is 4.17%.

2 RELATED WORK

In this section, we briefly review the most relevant works in indoor intrusion detection which can be grouped into three categories: video- and infrared-based approaches, RF-based approaches, and audio-based approaches.

2.1 Video- and Infrared-based Approaches

Video-based approaches [7-10] have been widely used to detect intrusion in public places. Cameras are installed to capture images or video for intruder recognition. Compared with other intrusion detection approaches, video-based approaches can detect intrusion, also retain full evidence. However, limited by visual angle, multiple cameras have to work together from different positions to cover an entire room and it fails if intruder is in NLOS area. In addition, video-based approaches are usually sensitive to light condition and may arise severe privacy concern when applied to home settings.

Infrared-based approaches [11-14] have been a mature intrusion detection solution for many years. These approaches can be further grouped into two categories. The first category leverages pyroelectric infrared sensor to capture infrared signals released by intruder. Limited by small sensing range, pyroelectric infrared sensors are usually deployed to monitor the small area around entrance. The second category leverages directional infrared sensor to detect transient moment when intruder block the line-of-sight between sender and receiver. To avoid underreporting, multiple sensors have to be deployed

in every possible entrance, such as door and window, to form a wireless sensor network. In addition, due to strong directionality, these sensors are required to be carefully installed by well-trained professionals. The complex deployment may prevent these systems from large-scale deployment in home settings.

2.2 RF-based Approaches

Radar-based approaches [15-17] share the same basic idea of extracting various features from the Doppler effect caused by walking, then detecting intrusion by matching feature variation pattern using machine learning algorithms. These approaches rely heavily on massive data for offline training. In addition, expensive hardware prevents large-scale deployment of these systems in home settings.

To build intrusion detection system friendly for home environment, researchers turn their attention to wide available commercial WiFi devices. In the early stage of WiFi sensing, Receive Signal Strength Indicator (RSSI) has been explored to detect intrusion [1,18-19,22-25,39]. The work [23,24] detect intrusion using a threshold to identify whether movement occurs. These approaches are sensitive to movement interference (e.g., curtain fluttering). The work [1,18-19,22,25,39] share same basic idea as radar-based approaches. They detect intrusion by extracting RSSI variation pattern from offline RSSI data using machine learning algorithms. These approaches heavily rely on massive offline data and suffer from poor environment adaptation ability.

Similarly, the work [2-4,20-21,26-29] detect intrusion by exacting the Channel State Information (CSI) variation pattern from offline CSI data using different machine learning algorithms. These approaches suffer from similar problems as RSSI-based and radar-based approaches. To overcome the limitations of the above approaches, Li et al. [30] propose to detect intrusion using a relatively robust feature CSI ratio, i.e., the ratio between dynamic CSI component and static CSI component. Furthermore, Li et al. [31] propose to detect intrusion by measuring Doppler shift embedded in CSI [40]. However, due to lack of mechanism to avoid interference, these two approaches are sensitive to movement interference such as object falling and curtain fluttering. The approach in [32] accurately detects intrusion by identifying the transient moment of an intruder entering a house with an accurate estimation of WiFi sensing boundary. Lin et al. [5] propose a CSI-EIH model to describe the effect of moving object's height to CSI amplitudes. Based on this model, the system can detect intrusion and avoid false alarm caused by pets. However, the system may raise false alarms if moving object is higher than the given height threshold. In addition to these shortcomings, CSI-based approaches have restriction on device location. They require that transmitter and receiver placed at two sides of intruder, else the performance declines significantly.

2.3 Audio-based Approaches

Audio-based approaches have recently attracted researchers' attention. Ultrasonic sensors are leveraged to build intrusion detection systems [33,34]. Due to strong directionality, ultrasonic sensors-based approaches suffer the same problem as in infrared-based approaches. Dissanayake et al [35] use the speaker and microphone embedded in smartphone to detect intrusion by identifying door opening and closing events based on Doppler shift. However, it is sensitive to location and orientation of smartphone because different location and orientation of smartphone may result in completely different Doppler shift. In addition, like both radar- and RSSI-based approaches, it also heavily relies on massive data for offline training. Microphone array has been used to detect intrusion [1,3]. However, these methods also heavily rely on massive data for offline training to cover all the possible conditions. Zieger et al [4] and Zu et al [38] proposed to extract various time and domain features of the data received by microphone array to identify intrusion. These approaches are all experience-based approaches lacking explainable theory. It leads to poor environment adaptation ability.

Differently, in this paper, we design and implement *AudioGuard*, an omnidirectional indoor intrusion detection system

using only a pair of speaker and microphone. *AudioGuard* detects intrusion by fully leveraging abundant multipath reflection in indoor environment to capture periodical Doppler shift caused by intruder's walking. It is able to detect both LOS and NLOS intrusions.

3 DOPPLER SHIFT CAUSED BY INTRUSION IN INDOOR ENVIRONMENT

3.1 Classical Doppler Effect

Doppler frequency shift is caused by relative movement between transmitter and receiver. In general, when a receiver moves towards a signal source, the frequency of the received signal increases, and vice-versa. Mathematically, the frequency of the received signal can be described as follows.

$$f' = \frac{c \pm v_r}{c \mp v_s} f \tag{1}$$

where f' is the received frequency; f is the transmitted frequency; c is the velocity of the wave in propagation medium; v_r is the radial velocity of the receiver relative to the medium (positive if the receiver is moving towards the source and negative otherwise); v_s is the radial velocity of the source relative to the medium (positive if the source is moving away from receiver and negative otherwise).

If the signal source and receiver are integrated to form an acoustic radar, then $v_r = v_s$. Plugging $\pm v_s = |\boldsymbol{v}| \cdot cos(\theta)$ ($\boldsymbol{v}$ and θ denote the walking speed of reflector and the angle between $\boldsymbol{v}$ and signal source, respectively) into Eq. 1, Doppler frequency shift Δf can be represented as:

$$\Delta f = f' - f = \left(\frac{2|\boldsymbol{v}| \cdot cos(\theta)}{c \mp |\boldsymbol{v}| \cdot cos(\theta)} \right) \cdot f \tag{2}$$

When $\boldsymbol{v}$ is much less than the velocity of sound c, we have $c \mp v_s \approx c$. Δf can be further simplified as:

$$\Delta f = \frac{2|\boldsymbol{v}| cos(\theta)}{c} f \tag{3}$$

The ideal model above assumes that the receiver only receives the signal reflected from the front of the moving reflector. Thus, the Doppler shift appears as the peak shift echo spectrum. As shown in Figure 1, when the reflector moves towards the transceiver with a speed of 1 m/s, the Doppler shift Δf apears as the peak shift of 283.4 Hz (the frequency of transmitting signal is 20 kHz and the sampling frequency is 48 kHz).

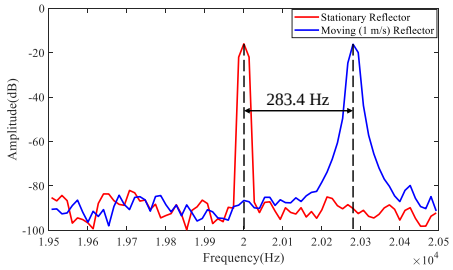

Figure 1: Classical Doppler shift caused by moving reflector

3.2 Doppler Shift Caused by Walking in Spectrum

Comparing with human body, the reflection area of static environment is much larger. In another word, the power of the multipath signal reflected from intruder is much lower than the power of the multipath signal reflected from the static environment. However, only the signals reflected from the moving object embeds with Doppler shift. It results that rather than changing the main peak of echo spectrum, the Doppler shift caused by intruder's walking appears as sidelobes of echo spectrum. Additionally, as shown in Figure 2(a), the change of the reflection path length of the signal reflected from the front and the back of intruder are always opposite, so they always introduce opposite Doppler shift (positive Doppler shift versus negative Doppler shift). Based above analysis we can finally derive that Doppler shift caused by walking always appears as two different shapes of sidelobes at two sides of the main peak of echo. Figure 2(b) shows the PSDs of echo (0.1 second) when intruder approaching and leaving the device (the frequency of transmitting signal is 20 kHz and the sampling frequency is 48 kHz). So, how to quantify the Doppler shift caused by the walking is challenging.

We consider a scenario where there are two people in a room and they are out of the sight of each other. For example, one is in bedroom and the other one is outside bedroom. One can still hear what the other says since the voice signals may be reflected from the static environment and propagate through multipath. Similarly, due to abundant acoustic multipath reflections in indoor environment, even the intruder is in NLOS areas, the microphone can still receive the signal indirectly reflected from intruder, thus, the echo still embedded with Doppler shift caused by intruder's walking.

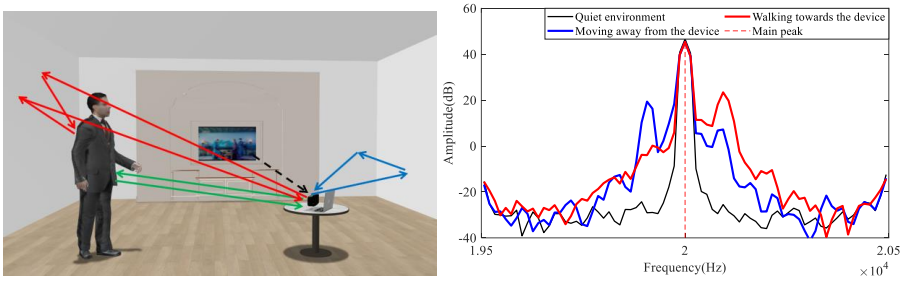

(a) (b)

Figure 2: Comparing the frequency resolution of FFT and the proposed method

3.3 Periodicity of the Doppler Shift Caused by Walking over Time

Figure 3(a) shows the time-frequency spectrum of the echo when intruder is walking away from the device (as shown in Figure 3(b)) and other interference (e.g., object falling, curtains fluttering, opening and closing door and chair sliding) happen.

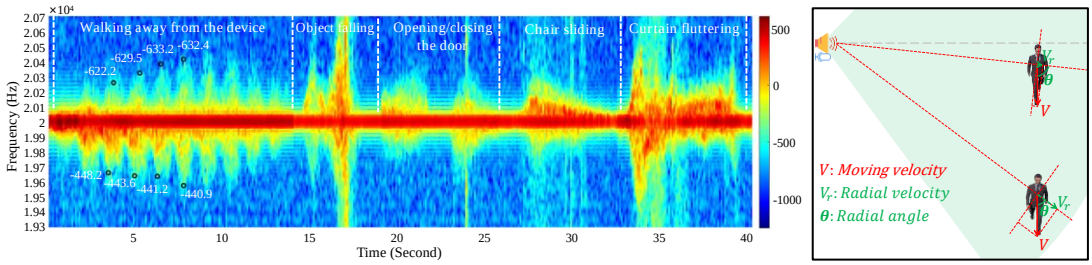

(a) (b)

Figure 3: Time-frequency spectrum of the echo when walking and other disturbance events happen.

From Figure 3(a), we observe that due to the periodic limbs swing during walking, the Doppler shift caused by walking

shows some periodicity, while Doppler shift caused by interference is aperiodic. So, our insight to detect intrusion is capturing the periodic Doppler shift sequence over time. However, from Figure 3(a) we also observe that the Doppler shift varies nonlinearly over time as radial angle and the distance varies during walking (shown in Figure 3(b)). Except for last two steps before stop, when the intruder is close to the device, the Doppler shift appears as low frequency shift but high power. When the intruder is far from the device, the Doppler shift appears as high frequency shift but low power. As shown in Figure 3(b), it is caused by the fact that when intruder is close to the device, the energy of the signal reflected from intruder is relative larger, while large radial angle leads to small radial velocity finally resulting in low frequency shift. When intruder is far from the device, the energy of the signal reflected from intruder is low, while small radial angle makes large radial velocity finally resulting in high frequency shift. So, how to cancel out the impact of radial angle and distance variation on the periodicity of Doppler shift is challenging.

4 SYSTEM DESIGN AND IMPLEMENTATION

4.1 System Framework

As shown in Figure 4, *AudioGuard* has three modules, namely Doppler effect extraction module, periodicity polarization module and intrusion detection module. The Doppler effect extraction module extracts Doppler shift using PSD difference vector. Periodicity polarization module firstly retains the segments that contain moving events, then polarizes the periodicity of the Doppler shift sequence. Intrusion detection module detects intrusion by measuring the periodicity of Doppler shift sequence over time.

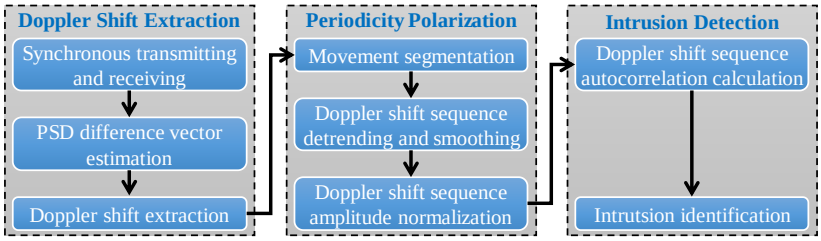

Figure 4: System framework.

4.2 Doppler Shift Extraction

AudioGuard continuously transmits a 20 kHz single frequency acoustic signal, which is inaudible for human, through a player. The microphone receives the echo synchronously with the sampling rate $f_s = 48\ kHz$. The length of the received frame is 0.1 second. To remove environment noise in echo, a band pass filter is adapted. Since the maximum walking velocity of human is approximately 4.3 m/s, according to Doppler shift formula [41], the maximum Doppler shift caused by intruder walking is about 500Hz. Therefore, the pass band of the filter is set as $[f_c - 500, f_c + 500]$.

As mentioned in Section 3, Doppler shift caused by intruder's walking motion appears as two different shapes of sidelobes at two sides of the main peak of echo spectrum. Traditional method, i.e., extracting main peak shift of PSD of echo, cannot be applied to capture Doppler shift under this condition. In this paper we capture Doppler shift using PSD difference vector.

PSD can be estimated using the Welch algorithm [6], which can significantly improve the variance characteristics of the power spectrum via overlap mechanism, also effectively reduce spectrum leakage via window function. Specifically, the PSD of one echo frame $x_r(n)$ is estimated as:

$$P(\omega_k) = \frac{1}{LN}\sum_{l=0}^{L-1}\left|\sum_{n=0}^{N-1} x_r(n + l \cdot M)w(n)\, e^{-jn\omega_k}\right|^2 \tag{4}$$

where ω_k is the digital angular frequency, which is defined as $\omega_k = k\Delta\omega = 2\pi k/N$. L is the number of overlapped segments. N is the length of each segment. M is the hop size. w is a window function with a length of N. As aforementioned, Doppler effect caused by walking appears at frequency band $f_c - 500 \le f_k \le f_c + 500$. According to the relationship between physical frequency f_k and digital angular frequency ω_k i.e., $\omega_k = 2\pi f_k/f_s$, where f_s is the sampling frequency, we can obtain the range of ω_k

$$\frac{2\pi(f_c - 500)}{f_s} \le \omega_k \le \frac{2\pi(f_c + 500)}{f_s} \tag{5}$$

Plugging $\omega_k = k\Delta\omega = 2\pi k/N$ into Eq. 5, we obtain the range of k

$$\frac{N(f_c - 500)}{f_s} \le k \le \frac{N(f_c + 500)}{f_s}$$

The minimum and maximum of k is

$$k_1 = \left\lceil\frac{N(f_c - 500)}{f_s}\right\rceil, k_H = \left\lfloor\frac{N(f_c + 500)}{f_s}\right\rfloor$$

Then, PSD difference vector of the echo frame at time t_i is defined as:

$$\boldsymbol{PD}_i = \left(diff^i_{k_1}, diff^i_{k_2}, \dots, diff^i_{k_m}, \dots, d^i_{iffk_H}\right), k_1 < k_2 < \cdots < k_H \tag{6}$$

where $diff^i_{k_m}$ is defined as:

$$diff^i_{k_m} = P_i(\omega_{k_m}) - P_{ref}(\omega_{k_m}) \tag{7}$$

P_i denotes the PSD of the echo frame at time t_i (refer to Eq. 4). P_{ref} denotes the reference PSD, which is the average PSD of the echo collected from current environment without any movement event. Every time when *AudioGuard* starting, it firstly runs the initializer to obtain reference PSD of current environment. Specifically, initializer continuously estimates echo PSD for 20 seconds, then calculates the average PSD value as reference PSD. During this process, any movement event is forbidden. If movement happens during getting reference PSD, the initializer automatically repeats getting reference PSD. Specifically, if the PSDs show obvious fluctuation, which can be easily observed from the variances of points in PSD over time, initializer runs again.

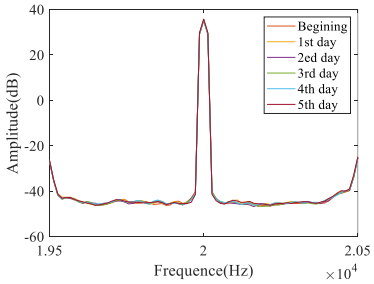

Figure 5: Reference PSDs over five days

We randomly record 20 seconds to get reference PSD for five days in same room without movement interference. Fig 5 shows the recorded reference PSD of each day. It can be observed that the reference PSDs are very similar. It indicates that if the environment does not change, we only need to get reference PSD for only one time.

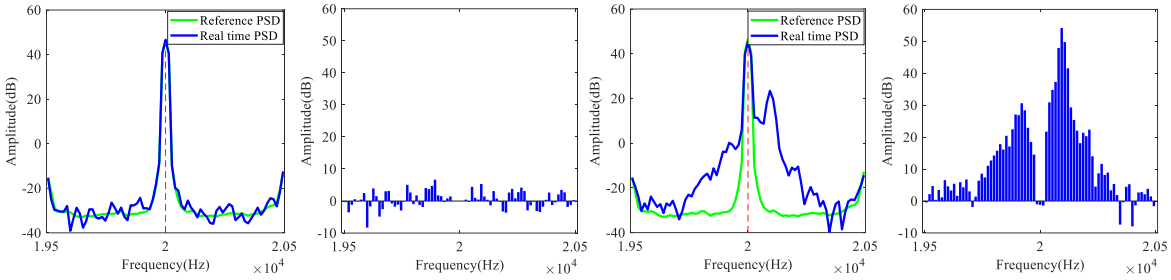

Figure 6: PSD difference vector.

Figure 6 (a) show the reference PSD and the PSD of one echo frame when there is no moving object. Figure 6 (b) shows the PSD difference vector derived from Figure 6 (a). Figure 6 (c) show the reference PSD and the PSD of one echo frame when one subject is walking. Figure 6 (d) shows the PSD difference vector derived from Figure 6 (c). Figure 7 shows all the samples of PSD difference vectors during one walking event containing seven steps. Even though during walking, the limbs swing is periodic, PSD difference vectors during walking do not show obvious periodicity. It is consistent with our analysis in Sec. 3.3.

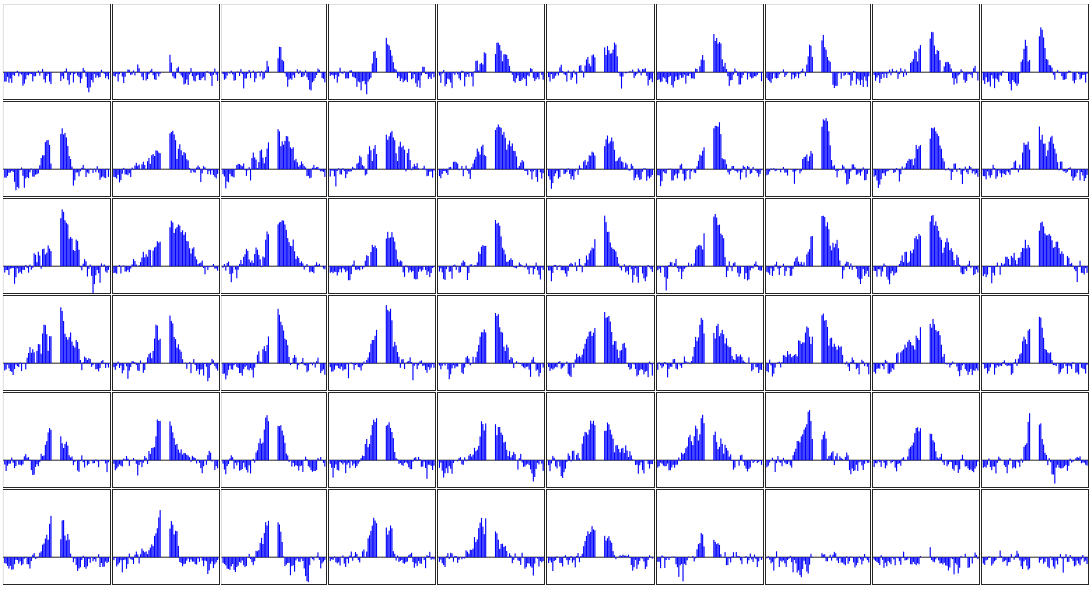

Figure 7: Samples of PSD difference vector during a walking event.

Finally, we quantify Doppler shift of the echo frame at time t_i as the first normal form of $\boldsymbol{PD}_i$, i.e.,

$$d_i = \|\boldsymbol{PD}_i\|_1 = \sum_{j=1}^{H} \left| diff_{k_j}^i \right| \tag{8}$$

4.3 Periodicity Polarization

Due to abundant acoustic multipath reflection in room environment, almost all the movement events (e.g., walking, door opening and closing, object falling, object sliding, and curtain fluttering) will introduce Doppler shift in echo. We have to firstly identify all the movement events, then identify intrusion among these movement events. According to Eq. 8, compare with the condition there is no moving object, when moving event happens, the value of d_i will be obviously larger due to Doppler shift. So, we can simply truncate the segments containing movement using a threshold. Specifically, to avoid the interference caused by system jitter, if d_i is larger than the threshold for 3 times continuously, we start to record d_i. Similarly, if d_i is smaller than the threshold for 3 times continuously, we stop to record d_i. Thus, each movement event can be segmented out and d_i over time is recorded. We call the recorded d_i over time as Doppler shift sequence. Figure 8 shows the Doppler shift sequence of different movement events.

We observe that the Doppler shift sequences caused by curtain fluttering and object sliding are aperiodic. Even though walking is periodic, Doppler shift sequence caused by walking (shown in Figure 8 (c)) shows weak periodicity. It is caused by the change of radial angle and the distance from intruder to device during walking (refer to Sec. 3.2). Too weak periodicity of Doppler shift sequence caused by walking will result in intrusion detection error. In order to improve intrusion detection accuracy, we intend to enhance the Doppler shift with weak periodicity while keep the periodicity of aperiodic Doppler shift sequence. In other words, we enlarge the periodicity difference between weak periodic Doppler shift sequence and aperiodic Doppler shift sequence. Thus, the intrusion can be easily detected as the Doppler shift sequence with strong periodicity.

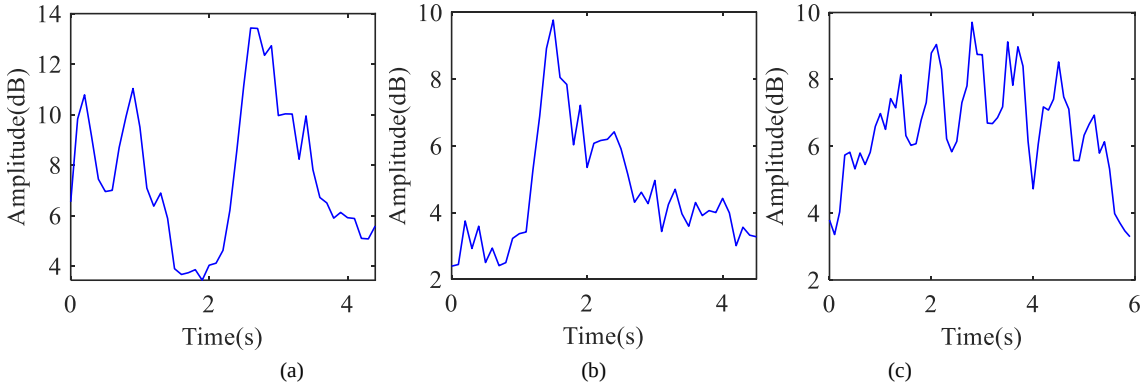

Figure 8: Doppler shift sequence of different movement events. (a) Curtain fluttering. (b) Object sliding. (c) Walking.

It's well known that strong periodicity simultaneously requires: 1) the shapes of the sequence during all periods are similar, and 2) the length of all the periods is almost constant. If any one of the requirements is not met, the signal will show weak even no periodicity. From Figure 6, we clearly see that, Doppler shift sequence caused by walking only meet the first requirement, while Doppler shift sequences caused by other aperiodic movement do not meet both two requirements. If we can enhance the similarity of sequence shape during each period while keep the length of original periods, Doppler shift sequence caused by walking will then meet both two requirements, while Doppler shift sequences caused by other aperiodic movement only meet the first requirement. Thus, the periodicity of Doppler shift sequence caused by walking will be significantly enhanced while the periodicity of Doppler shift sequence caused by other aperiodic movement will not be enhanced.

Periodicity polarization is designed to eliminate the difference of fluctuation amplitude in each period. Specifically, periodicity polarization process is composed of detrending, smoothing and amplitude normalization. Firstly, we extract the

polynomial trend of Doppler shift sequence and subtract it from Doppler shift sequence. Then, we smooth the detrended Doppler shift sequence to eliminate small burrs. Finally, we normalize the amplitude of Doppler shift sequence by eliminate the envelop of the sequence using Hilbert transform [37]. For detrended and smoothed Doppler shift sequence $\boldsymbol{d} = d_1, d_2, \dots d_i, \dots$, discrete Hilbert transform can be calculated by leveraging Discrete Fourier Transform (DFT) and Inverse Discrete Fourier Transform (IDFT).

$$\widehat{\boldsymbol{d}} = IDFT(\widehat{\boldsymbol{D}}) \tag{9}$$

where $\widehat{\boldsymbol{D}}$ is defined as:

$$\widehat{\boldsymbol{D}}(k) = \begin{cases} -j\boldsymbol{D}(k), k = \begin{cases} 1,2,\dots,N/2-1, when\ N\ is\ even \\ 1,2,\dots,(N-1)/2, when\ N\ is\ odd \end{cases} \\ j\boldsymbol{D}(k), k = \begin{cases} N/2+1,\dots,N-1, when\ N\ is\ even \\ (N+1)/2,\dots,N-1, when\ N\ is\ odd \end{cases} \end{cases} \tag{10}$$

where $\boldsymbol{D} = DFT(\boldsymbol{d})$. With $\widehat{\boldsymbol{d}}$, the envelope of $\boldsymbol{d}$, i.e., the amplitude of $\boldsymbol{d}$ over time can be calculated as

$$\boldsymbol{A}(n) = \sqrt{\boldsymbol{d}(n)^2 + \widehat{\boldsymbol{d}}(n)^2} \tag{11}$$

We then normalize $\boldsymbol{d}$ as

$$\boldsymbol{d}'(\boldsymbol{n}) = \frac{\boldsymbol{d}(\boldsymbol{n})}{\boldsymbol{A}(\boldsymbol{n})} \tag{12}$$

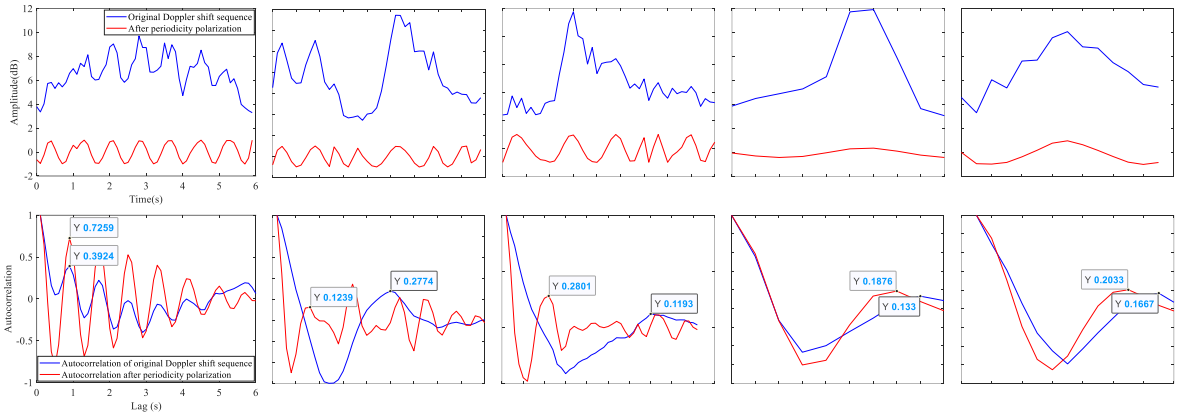

(a) Walking (b) Curtain fluttering (b) Object sliding (d) Object falling (e) Opening or closing door

Figure 9: Periodic polarization of the Doppler shift sequence of different moving events.

The subfigures in first line of Figure 9 show the original Doppler shift sequences (blue line) and the Doppler shift sequences after periodicity polarization (red line) of different moving events. Subfigures in second line of Figure 9 show the corresponding autocorrelations. Higher peak of the autocorrelation function means stronger periodicity. Comparing the autocorrelation of original Doppler shift sequences and that of the Doppler shift sequences after periodicity polarization, we can see that the periodicity of Doppler shift sequence of walking is significantly enhanced while the periodicities of other Doppler shift sequences are not enhanced obviously. It indicates that periodicity polarization is able to enlarge the periodicity difference between weak periodic Doppler shift sequence and aperiodic Doppler shift sequence.

4.4 Intrusion Detection

After periodicity polarization, intrusion can be easily detected as the Doppler shift sequence with strong periodicity. We measure the periodicity of Doppler shift sequence using autocorrelation function. The autocorrelation of the Doppler shift sequence after periodicity polarization $\boldsymbol{d}'$ is given by:

$$R_x(k) = \frac{c_k}{c_0} \tag{13}$$

where c_k is the auto-covariance of $\boldsymbol{S_i}$,

$$c_k = \frac{1}{N}\sum_{n=1}^{N-k}\left(\boldsymbol{d}'(n) - \bar{\boldsymbol{d}}'\right)\left(\boldsymbol{d}'(n+k) - \bar{\boldsymbol{d}}'\right), \quad k = 0,1,\dots,N-1 \tag{14}$$

From Figure 8, we observe that the autocorrelation function of periodic Doppler shift sequence looks like a sinusoid, but its amplitude decreases gradually, while the autocorrelation function of aperiodic Doppler shift sequence varies irregularly. Based on this characteristic, the rules are built as follows to judge whether intrusion happens. Suppose the coordinate value of first three peaks of the autocorrelation are (p_1, l_1), (p_2, l_2), (p_3, l_3), respectively, then the peak intervals are $PkIntevs = [l_1, l_2 - l_1, l_3 - l_2]$. If the following rules are satisfied, we judge intrusion happening.

$$\begin{cases} p_1 > PkThrd, and\ p_1 > p_2 > p_3, and \\ \dfrac{max(PkIntvs) - min(PkIntvs)}{mean(PkIntvs)} > IntvThrd \end{cases}$$

The first rule is designed to ensure that the shapes of the Doppler shift sequence within all periods are similar enough. The second rule ensures the lengths of all the periods are almost constant. The combination of the above two rules ensures that the detected Doppler shift is strong periodic. According to the experimental results in Sec 5.6 the threshold $PkThrd$ and $PkIntvs$ are suggested to set as 0.3~0.4 and 0.1~0.2, respectively.

5 EVALUATION

In this section, we conduct comprehensive experiments to evaluate *AudioGuard*. Firstly, we evaluate *AudioGuard* with LOS intrusion in office, laboratory, and home environment. We then test the performance for NLOS intrusion detection with 5 different settings in a real home environment. Finally, we evaluate its robustness. We test the impact of different transceivers, the variation of transceiver's location and orientation, different walking speed and various interference. Finally, we discuss the limitations of *AudioGuard*. The demo video of *AudioGuard* is available at https://tinyurl.com/4y44pdbk and https://youtu.be/iI-Pk4st75o.

5.1 Prototype Implementation

We implement *AudioGuard* on two different acoustic transceivers shown in Figure 10. Two transceivers have same commercial microphone (SAMSON MeteorMic, 16 bit, 48 kHz, 96 dB, 20Hz~20 kHz) but different speakers. The speaker in transceiver 1 is a commercial speaker (JBL Jembe, 6 Watt, 80 dB, 80Hz~20 kHz), while the speaker in transceiver 2 is a customized speaker (50 Watt, 96 dB, 1 kHz~40 kHz). We use transceiver 2 by default and compare the sensing range of transceiver 1 and transceiver 2 in Sec. 5.4.1. The acoustic transceiver is connected to a Lenovo laptop (Intel (R) Core (TM) i7-7500UCPU, 8GB RAM). The intrusion detection algorithm is implemented in MATLAB and runs in real-time. The frequency of transmitted signal is 20 kHz. The length of echo frame is 0.1 second.

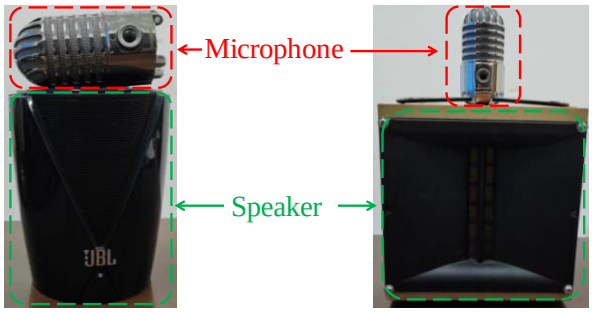

Figure 10: Two different transceivers

5.2 Evaluation for LOS Intrusion

As shown in Figure 11, we conduct LOS intrusion detection experiment in three different rooms, i.e., office (5.2m×3m), laboratory (8.4m×5.8m), and home (irregular shape, 148 m^2). In each environment, four subjects are recruited to enter the room or walk freely in the room for at least 100 times to test the miss report rate (i.e., False Negative Rate, FNR). Note that in the home setting, i.e., the third setting, to ensure the intrusion is in LOS, the subjects are required to walk in the areas highlighted as yellow.

Figure 11: LOS intrusion evaluation in three different rooms

Table 1: Experimental Result of LOS Intrusion Detection

Room	Number of experiments	Number of miss report	Miss report rate
Office	105	0	0%
Laboratory	121	0	0%
Home	110	0	0%

Table 1 shows the experimental result. We can see that *AudioGuard* accurately captures all the intrusion. Because there is no restriction on subjects' walking path, subjects change walking path dynamically during walking in part of the experiments. So, the result also indicates that within its sensing range (more than 120 m^2, refer to Sec. 5.5) *AudioGuard* is robust to intruder's location and walking direction.

5.3 Evaluation with NLOS Intrusion

We conduct NLOS intrusion detection experiment in a real home environment. Figure 12 shows the settings. The red circles mark the location of the transceiver. The areas highlighted as yellow are the places where intrusion happens. The settings ensure that the intrusion happens in NLOS area for transceiver.

In each setting, three subjects are recruited to walk in the yellow area freely for at least 100 times to test the miss report rate. Table 2 shows the experimental result. We can see that in first four settings *AudioGuard* can accurately capture

intrusions. However, in setting 5, *AudioGuard* fails because of the lack of effective reflected signal (i.e., the received multipath signal reflected from intruder). Similar results occur if the door is closed in settings 1, 2 and 4. In other words, if the effective reflected signal is blocked (e.g., door is closed) or the propagation path is too complex requiring too many times of reflection (e.g., setting 5), *AudioGuard* fails to detect intrusion.

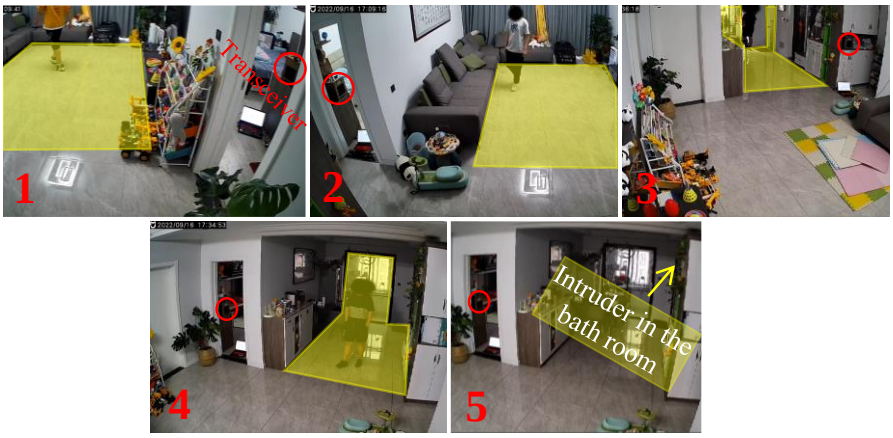

Figure 12: NLOS intrusion evaluation settings

Table 2: Experimental Result of NLOS Intrusion Detection

Setting Num.	Number of experiments	Number of miss report	Miss report rate
1	105	1	0.95%
2	121	2	1.65%
3	110	0	0
4	114	2	1.75%
5	100	87	87%

5.4 Robustness Evaluation

5.4.1 Impact of Different Transceiver

The sensing range is related to transmitting power. In the same environment, larger transmitting power results in larger sensing range. We conduct experiments in a laboratory (8.4m×6m×3.4m) and a large lobby (38m×8m×9m) to compare the sensing range of two different transceiver mentioned in Sec. 5.1. Specifically, as shown in Figure 13(a) and Figure 13(b), we divide the space of laboratory and lobby into 1×1 m^2 squares. To make full use of the space we firstly place the transceiver at one corner of the laboratory and lobby to measure the sensing range in front of the transceiver. Two subjects are asked to walk away from the transceiver at each square. The blue arrows and the dots in Figure 13(a), (b) denote the walking direction and the start point of walking. The red circles linked with arrow denote the location and orientation of transceiver in Figure 13 (a) ~ (f). If *AudioGuard* successfully detects the walking events, the square where the subject starts walking from is detectable, else the square is undetectable. To estimate the detectable area in the back of transceiver, the transceiver is placed facing towards the wall and the subject walk in the area in the back of transceiver.

The sensing range of transceiver 1 in the laboratory and lobby are shown in Figure 13(c) and Figure 13(d). The sensing range of transceiver 2 are shown in Figure 13(e) and Figure 13(f). The squares colored as green denote that *AudioGuard* successfully captures the walking events of both two subjects in these squares. The squares colored as yellow denote that

AudioGuard only captures the walking event of one subject and fails to detect the walking event of another subject in these squares. The squares colored as red denote that *AudioGuard* fails to capture the walking events of both two subjects in these squares.

We observe some interesting phenomena. Firstly, the sensing range of transceiver 2 is larger than that of transceiver 1, especially the sensing range in lobby. It reasonable that larger transmitting power of the transceiver result in larger sensing range. Secondly, comparing the sensing range of transceiver 1 in laboratory and lobby (as shown in Figure 13(c) and Figure 13(d)), we find that the space of the lobby is much larger than that of the laboratory, but the detectable area in the laboratory is larger than that in the lobby. However, the detectable area of transceiver 2 in the lobby (as shown in Figure 13(f)) is larger than that in the laboratory (as shown in Figure 13(e)). It indicates that the sensing range is related to both the transmitting power and the space of the environment. Larger rooms may have weaker multipath reflection and finally results in smaller sensing range.

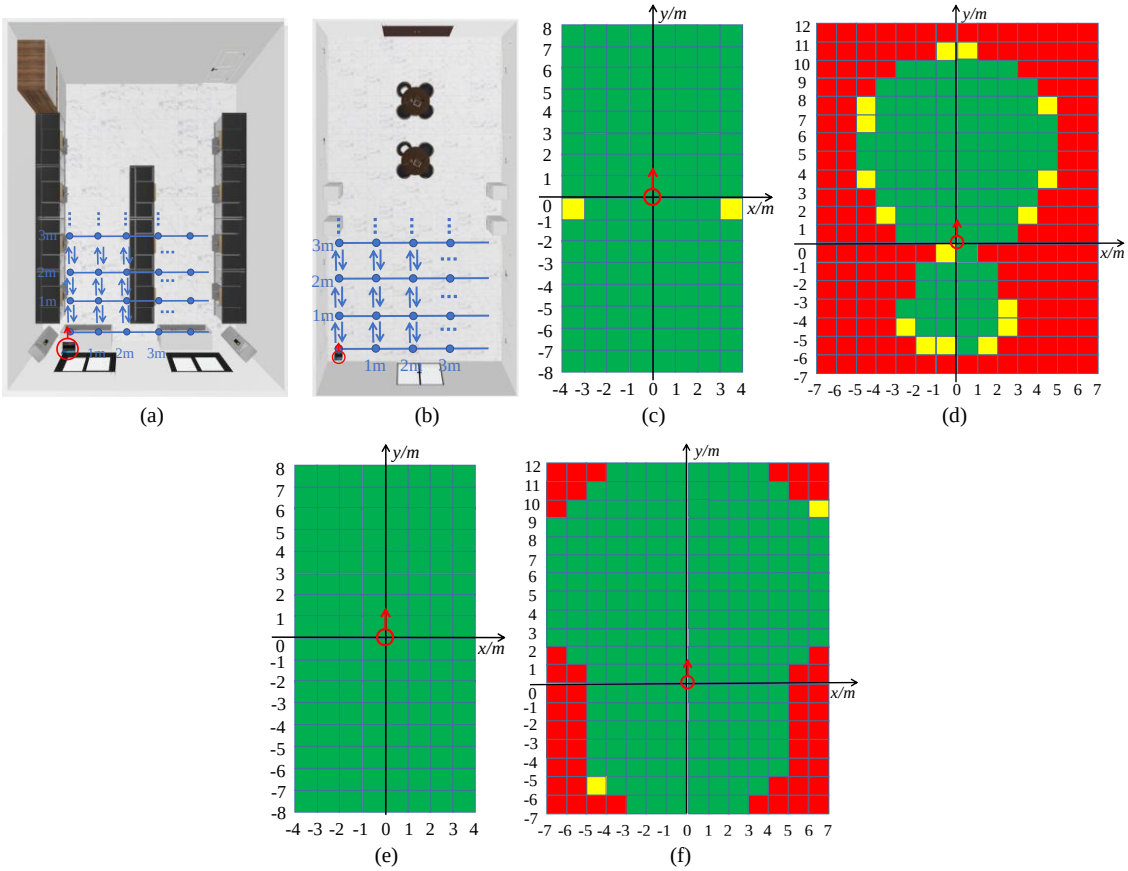

Figure 13: Sensing range of different transceiver in different environment

5.4.2 Impact of NLOS distance

From the experimental results in Sec 5.3, we know that the detectability of NLOS intrusion depends on the complexity of signal propagation path, which is closely related to NLOS distance (i.e., the distance along wall which blocks LOS between transceiver and intruder). In this section, we evaluate the impact of NLOS distance on intrusion detecting accuracy.

Specifically, the evaluation environment is shown in Figure 14(a). Two adjoining rooms (6m×3m) are connected by a door. The transceiver is placed in one room and the intrusion happens in the other room. The black arrows denote five walking paths that has different distance from the wall, 1 ~ 5 m. For each path, the one subject is recruited to walk 50 times. Figure 14(b) shows the miss report rates when subject walks along different paths. When the distance is larger than 3 m, the miss report rate increases significantly. Though increasing transmitting power may mitigate this problem, as NLOS distance increases, failing to detect intrusion is inevitable.

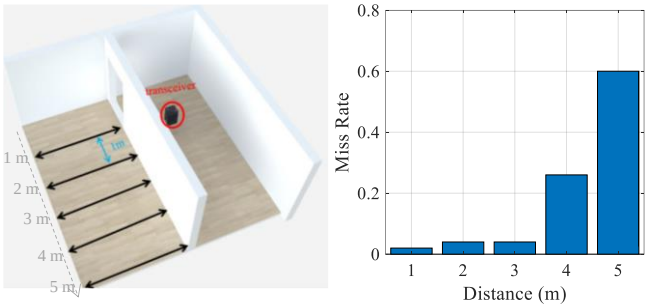

(a) Experimental settings (b)Miss report rate of each path

Figure14. Impact of NLOS distance

5.4.3 Impact of The Location and Walking Direction of Intruder

Adapting to the variation of intruder's location and walking direction is necessary for intrusion detection in real application environment. We now conduct experiments to test the impact of the location and walking direction of intruder on intrusion detection. As shown in Figure 15 (a), we divide the room (10m × 8m × 3.4m) into 8 areas with different shapes. The transceiver is placed at the center facing left (highlighted as the yellow circle with an arrow). 15 participants (including 5 females and 10 males) are recruited to walk in each area towards nine different directions (direction 9 is clockwise circle) to test the missing report rate. Each subject walks for two times towards each direction in each area. From the layout of the areas, areas 1 and 3, areas 7 and 5, areas 8 and 4 are all symmetric, respectively. So, we only need to test *AudioGuard* in the areas 1, 2, 6, 7 and 8.

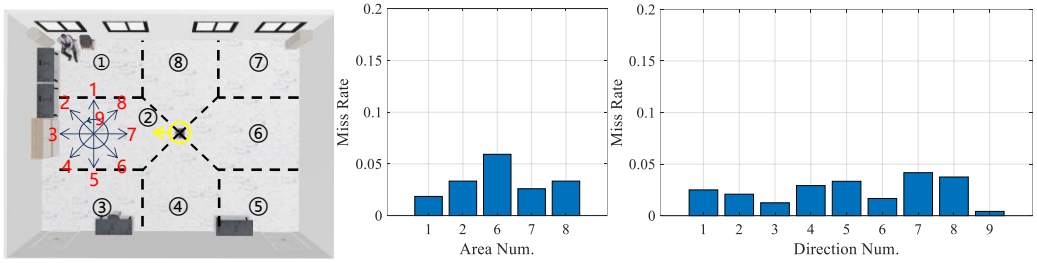

(a) The areas and walking directions (b) Missing report rate in each area (c) Miss report rate of each direction

Figure 15: Evaluation with Various Location and Walking Direction of Intruder

We summarize the experimental results from two aspects. Figure 15(b) shows the missing report rate in each area. We observe that except for area 6, the missing report rates of other areas are lower than 5%. The missing report rates of area 6 is slightly higher because area 6 is directly behind the transceiver. From the result of experiments in Sec. 5.4.2, the detectable area behind the transceiver is smaller than other orientations. In other words, the detectability of area 6 is

relatively lower than other areas. Figure 15(c) shows the statistics of missing report rate of each direction. We see that all the missing report rates are lower than 4%. In summary, the results indicate that *AudioGuard* is robust against intruder's location and walking direction.

5.4.4 Impact of The Location and Orientation of Transceiver

Robustness to the variation of transceiver's location and orientation is important for practical application. We place the transceiver randomly to test the missing report rate.

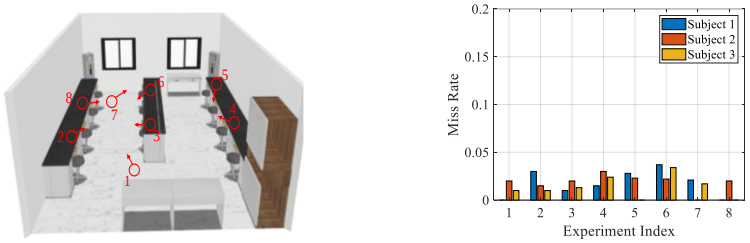

(a) Location and orientation of transceiver in each experiment. (b) Miss report rate of each experiment.

Figure 16: Evaluation with Various Location and Orientation of Transceiver

Figure 16(a) shows the transceiver's location and orientation in 8 experiments. In each experiment, 3 subjects are recruited to enter the room or walk freely in the room (8.4m×5.8m). Figure 16(b) shows the miss report rate in each experiment. We observe that the miss report rates are all lower than 4%. It indicates that *AudioGuard* is robust against the variation of transceiver's location and orientation.

5.4.5 Impact of Walking Speed

Different people have different walking speed. It's necessary to test the robustness against different speed. 5 subjects are recruited to evaluate the miss report rate of *AudioGuard*. Subjects are required to walk at four speed levels: 0.5~0.8 m/s, 0.8~1.2 m/s, 1.5~2 m/s and 2~3 m/s. There is no restriction for walking path. The experimental result is shown in Figure 17. We observe that there is no miss report when the walking speed is lower than 1.2 m/s, which is a normal walking speed. When walking fast, i.e., the speed reaches 1.5 ~ 2 m/s, the miss report rate is still lower than 10%. When running, i.e., the speed reaches 2 ~ 3 m/s, the miss report rate increases significantly. It is reasonable that when running the stride frequency is about 2 ~ 4 steps per second, i.e., 2 ~ 4 Hz. As mentioned in Sec. 4.2, the length of the received echo frame is 0.1 second. It means that the sampling rate of Doppler shift is $1/0.1 = 10$ Hz, which is too low to clearly depict the periodicity of Doppler shift sequence caused by running. Thus, when running, the miss report rate increases significantly.

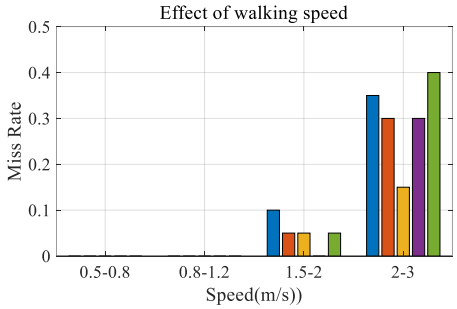

Figure 17: Effect of walking speed

5.4.6 Impact of Interference

We now conduct experiment to test the robustness against noise interference (talking, knocking door, playing music) and movement interference (opening or closing door and window, object falling, curtain fluttering).

As shown in Table 3, there are 6 different interferences, and each interference is repeated for 20 times. Totally 120 times interference randomly mixed with an equal number of walking are used to test both the miss report rate and false alarm rate (i.e., False Positive Rate, FPR). Figure 18 shows the confusion matrix.

Table 3: Interference

Interference	Number of experiments
Talking	20
Knocking door	20
Playing music	20
Opening or closing door and window	20
Object falling	20
Curtain fluttering	20

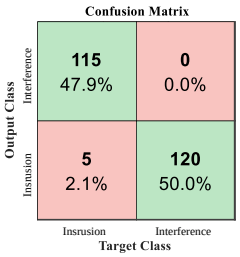

Figure 18: Confusion matrix

5.4.7 Impact of Key Thresholds

We now evaluate the impact of two key thresholds, i.e., $kThrd$ and $PkIntvs$ (refer to Sec. 4.4) on miss report rate and false alarm rate. We know that common ambient noise cannot incur false alarming as they do not incur Doppler shift. So, in this experimental, we only add three kind of movement events (including opening or closing door and window, object falling and curtain fluttering) as interference. Specifically, intrusion and movement interference randomly happen for 100 times and 60 times respectively. Figure 19 (a) shows the ROC curve when $PkIntvs = 0.1$ and $kThrd$ varies from 0.1 to 0.6 with a step of 0.1. Figure 19 (a) shows the ROC curve when $kThrd = 0.3$ and $PkIntvs$ varies from 0 to 0.2 with a step of 0.05. According to above results, $PkThrd$ and $PkIntvs$ are suggested to set as 0.3~0.4 and 0.1~0.2, respectively.

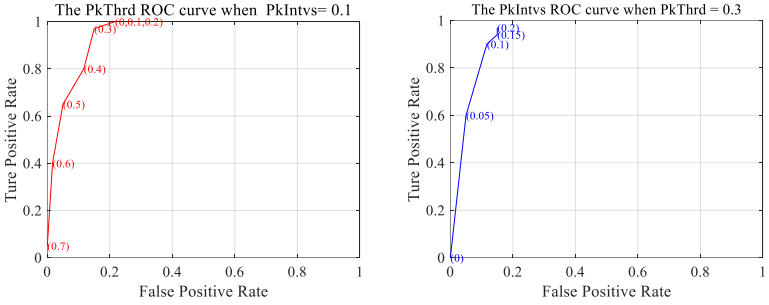

Figure 19: Impact of two key thresholds, $PkThrd$ and $PkIntvs$

5.5 Consuming Time Evaluation

In this section, we conduct an experiment to test the computational overhead of *AudioGuard*. As presented in Sec. 4.2, the length of the received audio frame by the microphone is 0.1 second. The iteration cycle of *AudioGuard* is equal to the length of audio frame. To ensure *AudioGuard* runs in real time, the consuming time of signal processing have to be shorter than 0.1 second, else frame drop occurs. We test the consuming time of the signal processing of *AudioGuard* under three different settings: 1) no any movement happens, 2) movement interference happens, 3) intrusion happens. For each setting, *AudioGuard* iterates for 1000 times and we record the consuming time. Table 4 shows the statistics of the consuming time under three settings. We observe that the maximums of consuming time of signal processing under three settings are all smaller than 0.049 second, which is far less than the upper bound 0.1 second.

Table 4: System run-time and latency

	Number of Iterations	Mean	Variance	Minimum	Maximum
No any movement	1000	0.027	0.000	0.025	0.036
Movement interference happens	1000	0.027	0.000	0.025	0.041
Intrusion happens	1000	0.028	0.003	0.026	0.049

5.6 Discuss

We now discussion limitations in the current implementation.

1) *AudioGuard* can only detect the intrusion caused by single intruder. It cannot detect intrusion caused by multiple intruders. *AudioGuard* detects intrusion by measuring the periodicity of Doppler shift. When multiple intruders walk simultaneously, their different stride frequencies (non-multiple) incur aperiodic Doppler shift, which will be regarded as interference by *AudioGuard*. A promising way to tackle this problem is decomposing Doppler shift sequence using the method such as time-frequency domain analysis and independent component analysis (ICA).

2) *AudioGuard* is sensitive to periodical movement interference. As mentioned in Sec. 3.3, the basic idea of *AudioGuard* is to capture the periodical Doppler shift sequence, when periodical movement interference happens, *AudioGuard* may experience false alarms. It is worth noting that the periodical sound interference (such as the sound of knocking door, the sound of footsteps outside the room, the sound of periodical music, etc.) will not result in false alarm. Because pure sound will not introduce Doppler shift. To avoid periodical movement interferences, other features of Doppler shift need to be extracted to distinguish the category of moving object.

3) *AudioGuard* may miss the intrusion when intruder is running. As mentioned in Sec. 5.4.5, running will blur the periodicity of Doppler shift sequence, which may finally lead to miss report.

4) *AudioGuard* may miss the intrusion in NLOS condition if the reflected signal is seriously blocked. As mentioned in Sec. 5.3, if the reflected signal is completely blocked by door, *AudioGuard* fails. Additionally, if the propagation path between the area where the transceiver locates and the area where the intruder locates is too complex requiring too many times of reflection, *AudioGuard* fails. This problem may be solved by exploiting room Channel Impulse Response (CIR) estimation, which is able to quantify both the time delay and amplitude attenuation of the multipath signals. CIR is more sensitive to movement than Doppler effect in indoor environment.

ACKNOWLEDGMENTS

The authors would like to express their special appreciation to all the volunteers for participating in our experiments. This work is supported in part by the Key Research and Development Project in Shaanxi Province of China (2023-YBGY-257),

Shaanxi Key Industry Innovation Chain Project (2023-ZDLNY-69) and Yangling Livestock Industry Innovation Center Double-chain Fusion Project (2022GD-TSLD-46).

REFERENCES

[1] Young-Keun Choi, Ki-Man Kim, Ji-Won Jung, Seung-Yong Chun and Kyu-Sik Park. 2005. Acoustic intruder detection system for home security. IEEE Transactions on Consumer Electronics 51, 1 (Feb 2005), 130–138. http://doi.org/10.1109/TCE.2005.1405710

[2] Yanni Yang, Jiannong Cao, Xiulong Liu and Xuefeng Liu. 2020. Door-Monitor: Counting In-and-Out Visitors With COTS WiFi Devices. IEEE Internet of Things Journal 7,3 (Mar 2020),1704–1717. http://doi.org/10.1109/JIOT.2019.2953713

[3] Yuepeng Li, Jun Yang, Xiaodong Li and Jing Tian. 2006. Ultrasonic intruder detection system for home security. Intelligent Control and Automation. Vol. 344. Springer, Berlin, Heidelberg. http://doi.org/10.1007/978-3-540-37256-1_143

[4] Zieger, Christian, Alessio Brutti and Piergiorgio Svaizer. 2009. Acoustic based surveillance system for intrusion detection. 2009 Sixth IEEE International Conference on Advanced Video and Signal Based Surveillance. IEEE, Genova, Italy, 314–319. http://doi.org/10.1109/AVSS.2009.49

[5] Yuxiang Lin, Y Gao, Bingji Li and Wei Dong. 2020. Revisiting Indoor Intrusion Detection With WiFi Signals: Do Not Panic Over a Pet!. IEEE Internet of Things Journal 7, 10 (Oct 2020), 10437–10449. http://doi.org/10.1109/JIOT.2020.2994101

[6] Tianben Wang, Daqing Zhang, Leye Wang, Yuanqing Zheng, Tao Gu, Bernadette Dorizzi and Xingshe Zhou.2019. Contactless Respiration Monitoring Using Ultrasound Signal With Off-the-Shelf Audio Devices. IEEE Internet of Things Journal 6, 2 (Apr 2019), 2959–2973. http://doi.org/10.1109/JIOT.2018.2877607

[7] G Milanesi, A Sarti and S Tubaro. 2002. Real-time video analysis for intrusion detection in indoor environments. 2002 11th European Signal Processing Conference. IEEE, Toulouse, France, 1–4.

[8] Manoranjan Paul, Shah M E Haque and Subrata Chakraborty. 2013. Human detection in surveillance videos and its applications-a review. EURASIP Journal on Advances in Signal Processing 2013 176 (Nov 2013), 1–16. http://doi.org/10.1186/1687-6180-2013-176

[9] Bo-Wei Chen, Chen-Yu Chen and Jhing-Fa Wang. 2013. Smart homecare surveillance system: Behavior identification based on state-transition support vector machines and sound directivity pattern analysis. IEEE Transactions on Systems, Man, and Cybernetics: Systems 43.6 (Nov 2013), 1279–1289. http://doi.org/ 10.1109/TSMC.2013.2244211

[10] Rashmiranjan Nayak, Mohini Mohan Behera, Umesh Chandra Pati and Santos Kumar Das. 2019. Video-based Real-time Intrusion Detection System using Deep-Learning for Smart City Applications. 2019 IEEE International Conference on Advanced Networks and Telecommunications Systems (ANTS) . IEEE, Goa, India, 1–6. http://doi.org/10.1109/ANTS47819.2019.9117960

[11] Ju Han and B.Bhanu. 2005. Human activity recognition in thermal infrared imagery. 2005 IEEE Computer Society Conference on Computer Vision and Pattern Recognition (CVPR'05)-Workshops. IEEE, San Diego, CA, USA, 17-17. http://doi.org/10.1109/CVPR.2005.469

[12] Yun Li, Yong Song, Yufei Zhao,Shangnan Zhao, Xu Li, Lin Li and Songyuan Tang. 2017. An infrared target detection algorithm based on lateral inhibition and singular value decomposition.Infrared Physics & Technology 85 (Sept 2017), 238–245. http://doi.org/10.1016/j.infrared.2017.07.005

[13] Khirod Chandra Sahoo and Umesh Chandra Pati. 2017. IoT based intrusion detection system using PIR sensor. 2017 2nd IEEE International Conference on Recent Trends in Electronics, Information & Communication Technology (RTEICT) . IEEE, Bangalore, India, 1641–1645. http://doi.org/ 10.1109/RTEICT.2017.8256877

[14] Sami Aldalahmeh, Amer Hamdan, Mounir Fhogho and Des McLernon. 2016. Enhanced-range intrusion detection using pyroelectric infrared sensors. 2016 Sensor Signal Processing for Defence (SSPD) . IEEE, Edinburgh, UK, 1–5. http://doi.org/10.1109/SSPD.2016.7590597

[15] Michael Otero. 2005. Application of a continuous wave radar for human gait recognition. Signal Processing, Sensor Fusion, and Target Recognition XIV 5809. (May 2005), 538–548. Orlando, Florida. http://doi.org/10.1117/12.607176

[16] Milenko S. Andrić, Boban P. Bondžulić, Dimitrije M. Bujaković and Srđan T. Mitrović. 2011.Analysis of Radar Doppler Echoes from Various Ground Moving Targets. International Conference on Aerospace Sciences and Aviation Technology, 1–11. http://doi.org/10.21608/ASAT.2011.23243.

[17] Fioranelli, Francesco, Matthew Ritchie, and Hugh Griffiths. 2015. Multistatic human micro-Doppler classification of armed/unarmed personnel. IET Radar, Sonar & Navigation 9.7 (Aug 2015), 857–865. http://doi.org/10.1049/iet-rsn.2014.0360

[18] Mu Zhou, Yaoping Li, Liangbo Xie and Wei Nie. 2019. Maximum Mean Discrepancy Minimization Based Transfer Learning for Indoor WLAN Personnel Intrusion Detection. IEEE Sensors Letters 3, 8 (Aug 2019), 1–4. http://doi.org/10.1109/LSENS.2019.2932099

[19] Mu Zhou, Yaoping Li, Xiaoge Huang, Qianlin Pu and Hui Yuan. 2019. Indoor WLAN Intrusion Detection Using Intra-class Transfer Learning with Low Effort.2019 IEEE 30th Annual International Symposium on Personal, Indoor and Mobile Radio Communications (PIMRC). IEEE, Istanbul, Turkey, 1–6. http://doi.org/10.1109/PIMRC.2019.8904445

[20] Jiguang Lv, Dapeng Man, Wu Yang, Xiaojiang Du and Miao Yu. 2017. Robust WLAN-based indoor intrusion detection using PHY layer information. IEEE Access 6 (Dec 2017), 30117–30127, http://doi.org/10.1109/ACCESS.2017.2785444

[21] Jiguang Lv, Wu Yang, Liangyi Gong, Dapeng Man and Xiaojiang Du. 2016. Robust WLAN-Based Indoor Fine-Grained Intrusion Detection. 2016 IEEE Global Communications Conference (GLOBECOM) . IEEE, Washington, DC, USA, 1–6. https://doi.org/10.1109/GLOCOM.2016.7842238

[22] Mu Zhou, Yixin Lin, Nan Zhao, Qing Jiang, Xiaolong Yang and Zengshan Tian. 2020. Indoor WLAN Intelligent Target Intrusion Sensing Using Ray-Aided Generative Adversarial Network. IEEE Transactions on Emerging Topics in Computational Intelligence 4, 1 (February 2020), 61–73. https://doi.org/10.1109/TETCI.2019.2892748

[23] Yue Jin, Zengshan Tian, Mu Zhou, Ze Li and Zhenyuan Zhang. 2018. A Whole-Home Level Intrusion Detection System using WiFi-enabled IoT. 2018 14th International Wireless Communications & Mobile Computing Conference (IWCMC) . IEEE, Limassol, Cyprus, 494–499.

https://doi.org/10.1109/IWCMC.2018.8450442

[24] Mohamed Hadi Habaebi, Mahamat Mahamat Ali, M.M.Hassan, M.S.Shoib, A.A.Zahrudin, A.A.Kamarulzaman, W.S. WanAzhan and Md. RafiqulIslam. 2015. Development of physical intrusion detection system using Wi-Fi/ZigBee RF signals. Procedia Computer Science 76 (2020), 547–552. https://doi.org/10.1016/j.procs.2015.12.342

[25] Zengshan Tian, Xiangdong Zhou, Mu Zhou, Shuangshuang Li and Luyan Shao. 2015. Indoor device-free passive localization for intrusion detection using multi-feature PNN. 2015 10th International Conference on Communications and Networking in China (ChinaCom) . IEEE, Shanghai, 272–277. https://doi.org/10.1109/CHINACOM.2015.7497950

[26] Enjie Ding, Xiansheng Li, Tong Zhao, Lei Zhang and Yanjun Hu. 2018. A robust passive intrusion detection system with commodity WiFi devices. Journal of Sensors. https://doi.org/10.1155/2018/8243905

[27] Chong Han, Qingqing Tan, Lijuan Sun, Hai Zhu, and Jian Guo. 2018. Csi frequency domain fingerprint-based passive indoor human detection. Information 9, 4 (April 2018), 95–108. https://doi.org/10.3390/info9040095

[28] Dan Wu, Youwei Zeng, Ruiyang Gao, Shengjie Li, Yang Li, Rahul C Shah, Hong Lu and Daqing Zhang. 2021. WiTraj: Robust Indoor Motion Tracking with WiFi Signals. IEEE Transactions on Mobile Computing (December 2021), 1–1. https://doi.org/10.1109/TMC.2021.3133114

[29] Zengshan Tian, Yong Li, Mu Zhou and Ze Li. 2018. WiFi-Based Adaptive Indoor Passive Intrusion Detection. 2018 IEEE 23rd International Conference on Digital Signal Processing (DSP) . IEEE, Shanghai, China, 1–5. https://doi.org/10.1109/ICDSP.2018.8631613

[30] Shengjie Li, Xiang Li, Kai Niu, Hao Wang, Yue Zhang and Daqing Zhang. 2017. Ar-alarm: An adaptive and robust intrusion detection system leveraging csi from commodity wi-fi. International conference on smart homes and health telematics. Springer, Cham, 211–223. https://doi.org/10.1007/978-3-319-66188-9_18

[31] Shengjie Li, Zhaopeng Liu, Yue Zhang, Xiaopeng Niu, Leye Wang and Daqing Zhang. 2019. A real-time and robust intrusion detection system with commodity wi-fi. Adjunct Proceedings of the 2019 ACM International Joint Conference on Pervasive and Ubiquitous Computing and Proceedings of the 2019 ACM International Symposium on Wearable Computers (UbiComp/ISWC'09) . 316–319. https://doi.org/10.1145/3341162.3343789

[32] Shengjie Li, Zhaopeng Liu, Yue Zhang, Qin Lv, Xiaopeng Niu, Leye Wang and Daqing Zhang. 2020. WiBorder: Precise Wi-Fi based Boundary Sensing via Through-wall Discrimination. Proceedings of the ACM on Interactive, Mobile, Wearable and Ubiquitous Technologies 4, 3 (September 2020), 1–30. https://doi.org/10.1145/3411834

[33] Omar Sonbul and Alexander N. Kalashnikov. 2013. Low cost ultrasonic wireless distributed security system for intrusion detection. 2013 IEEE 7th International Conference on Intelligent Data Acquisition and Advanced Computing Systems (IDAACS) . IEEE, Berlin, Germany, 235–238. https://doi.org/10.1109/IDAACS.2013.6662679

[34] R Unni and U.C Pati. 2018. PC Based Ultrasonic Intrusion Detection System. 2018 International Conference on Communication and Signal Processing (ICCSP) . IEEE, Chennai, India, 942–947. https://doi.org/10.1109/ICCSP.2018.8524262

[35] Thilina Dissanayake, Takuya Maekawa, Daichi Amagata and Takahiro Hara. 2018. Detecting Door Events Using a Smartphone via Active Sound Sensing. Proceedings of the ACM on Interactive, Mobile, Wearable and Ubiquitous Technologies 2, 4 (December 2018), 1–26. https://doi.org/10.1145/3287038

[36] https://safeatlast.co/blog/burglary-statistics/

[37] Feldman, Michael. 2011. Hilbert Transform Applications in Mechanical Vibration: Feldman/Hilbert Transform Applications in Mechanical Vibration. John Wiley & Sons.

[38] Xingshui Zu, Feng Guo, Jingchang Huang, Qin Zhao, Huawei Liu, Baoqing Li and Xiaobing Yuan. 2017. Design of an acoustic target intrusion detection system based on small-aperture microphone array. Sensors 17, 3 (March 2017), 514. https://doi.org/10.3390/s17030514

[39] Chia-How Lin and Kai-Tai Song. 2013. Probability-based location aware design and on-demand robotic intrusion detection system. IEEE Transactions on Systems, Man, and Cybernetics: Systems 44, 6 (June 2013), 705–715. https://doi.org/10.1109/TSMC.2013.2277691

[40] Kai Niu, Fusang Zhang, Xuanzhi Wang, Qin Lv, Haitong Luo and Daqing Zhang. 2021. Understanding WiFi signal frequency features for position-independent gesture sensing. IEEE Transactions on Mobile Computing 21, 11 (March 2021), 4156–4171. https://doi.org/10.1109/TMC.2021.3063135

[41] Tianben Wang, Daqing Zhang, Leye Wang, Yuanqing Zheng, Tao Gu, Bernadette Dorizzi and Xingshe Zhou. Contactless respiration monitoring using ultrasound signal with off-the-shelf audio devices. IEEE Internet of Things Journal 6, 2 (April 2018), 2959–2973. https://doi.org/10.1109/JIOT.2018.2877607